AGU PUBLICATIONS

JGR

Journal of Geophysical Research: Atmospheres

RESEARCH ARTICLE
10.1002/2014JD022849

Key Points:
- Black carbon (BC) climate interactions vary significantly with altitude
- Negative forcing from BC semidirect effects opposes its direct radiative effect
- Semidirect effects are critical for BC temperature and precipitation impacts

Correspondence to:
B. H. Samset,
b.h.samset@cicero.oslo.no

Citation:
Samset, B. H., and G. Myhre (2015), Climate response to externally mixed black carbon as a function of altitude, *J. Geophys. Res. Atmos.*, *120*, 2913–2927, doi:10.1002/2014JD022849.

Received 13 NOV 2014
Accepted 12 MAR 2015
Accepted article online 18 MAR 2015
Published online 10 APR 2015

Climate response to externally mixed black carbon as a function of altitude

B. H. Samset[1] and G. Myhre[1]

[1]Center for International Climate and Environmental Research—Oslo, Oslo, Norway

Abstract The climate response to the presence of black carbon (BC) aerosol at a given altitude in the atmosphere is investigated using a global circulation model. The vertical dependence of the efficiency with which BC exerts radiative forcing (RF) through the direct aerosol effect has previously been extensively studied. Here we use the Community Atmosphere Model version 4 atmospheric component of the National Center for Atmospheric Research Community Earth System model version 1.03 to calculate the three-dimensional response to a BC layer inserted at various altitudes. Simulations have been performed both for fixed sea surface temperatures and using a slab ocean setup to include the surface temperature response. We investigate the vertical profiles of RF exerted per gram of externally mixed BC due to both the direct and semidirect aerosol effects. Associated changes in cloud cover, relative humidity, and precipitation are discussed. The precipitation response to BC is decomposed into a fast, stability-related change and a slow, temperature-driven component. We find that while the efficiency of BC to exert positive RF due to the direct effect strengthens with altitude, as in previous studies, it is strongly offset by a negative semidirect effect. The net radiative perturbation of BC at top of atmosphere is found to be positive everywhere below the tropopause and negative above. The global, annual mean precipitation response to BC, after equilibration of a slab ocean, is found to be positive between the surface and 900 hPa but negative at all other altitudes.

1. Introduction

Black carbon (BC) aerosols, a class of carbonaceous particles emitted through incomplete combustion [*Bond et al.,* 2013], are known to absorb incoming solar radiation and may exacerbate global warming. This climate impact comes both through the direct interaction of BC with sunlight (termed as the aerosol direct effect), the impact of BC presence on cloud albedo and lifetime (termed as aerosol indirect effects), the effect that local warming from BC presence has on clouds through changes in atmospheric stability and humidity (termed as the semidirect effect), as well as albedo modification through deposition of BC on snow and ice. The total radiative forcing from BC over the industrial era (1750–2005) was recently evaluated to be +0.71 W m^{-2}, with 90% uncertainty bounds of (+0.08, +1.27) W m^{-2} [*Bond et al.,* 2013]. Of this, the radiative forcing (RF) from the direct effect, due to BC from burning of fossil and biofuels, was found to be +0.51 W m^{-2}. The Intergovernmental Panel on Climate Change Fifth Assessment Report evaluated the same quantity to be +0.4 (+0.05,+0.8) W m^{-2} [*Boucher et al.,* 2013]. *Bond et al.* [2013] further evaluated the semidirect effect of anthropogenic BC to be −0.1 (−0.3,+0.1) W m^{-2}. The large uncertainty on the latter range highlights the urgent need for improved understanding of this mode of BC climate interaction.

In general, aerosols, and their direct and indirect impacts on the global radiation budget, constitute a major source for uncertainty in our constraints on past and future anthropogenic climate change. Uncertainties exist in both emissions and the resulting impacts for all aerosol species [*Boucher et al.,* 2013]. While estimates of the mean BC direct RF from models and observations have recently converged [*Myhre*, 2009], model studies generally yield lower uncertainty ranges than observational estimates [see, e.g., *Samset et al.,* 2014].

It is therefore of crucial importance to understand the details of the climate impact of each individual aerosol species, as part of the effort to reduce overall uncertainties in climate projections.

For BC, one particularly large source of uncertainty comes from the sensitivity of its various climate impacts to vertical location. Several model studies have showed that the direct RF efficiency of BC strongly increases with altitude, due to radiative interactions with clouds, other aerosols, and ambient air [see, e.g., *Samset and Myhre*, 2011; *Vuolo et al.,* 2014; *Zarzycki and Bond*, 2010]. While these studies agree qualitatively, there are differences in the predicted absolute forcing strength of BC.

The total impact of BC as a function of altitude, taking into account dynamical effects on clouds, atmospheric stability, humidity, and precipitation, is less well constrained. Notably, some model studies have perturbed BC at various regions and/or altitudes and tracked resulting impacts through global circulation models [*Ban-Weiss et al.,* 2011; *Flanner*, 2013; *Hansen et al.,* 1997, 2005; *Hodnebrog et al.,* 2014; *Kvalevag et al.,* 2013; *Sand et al.,* 2013]. Broadly, they find a surface warming for BC injected at most locations, except for higher altitudes over the polar regions. Here surface cooling has been reported in several studies. However, there is considerable intermodel variability in the results.

Further, the present vertical profile of BC concentration is poorly constrained, both by observations [*Schwarz et al.,* 2013] and models [*Koch et al.,* 2009]. It was recently found that model diversity in predicted BC profiles may cause 20–50% of intermodel variability in estimates of the direct BC forcing over the industrial era [*Samset et al.,* 2013], even when explicitly removing model differences in forcing efficiencies. The differences are mainly due to BC lifetime, long range transport, wet removal, convective lifting, and other processes being treated differently by models [*Allen and Landuyt*, 2014; *Kipling et al.,* 2013; *Koch et al.,* 2009; *Samset et al.,* 2014].

There is a clear need for further model estimates of the vertical dependence of both the direct forcing efficiency and impacts on clouds and precipitation as input to ongoing discussions about reductions of BC emissions as a possible climate mitigation strategy. At present, both the resulting changes to atmospheric loads and vertical profiles from such a reduction are inadequately constrained as are the actual impacts from changes at various altitudes.

In the present study, we have used the National Center for Atmospheric Research (NCAR) Community Atmosphere Model version 4 (CAM4) to investigate the climate impact of BC as a function of altitude. We will show how a BC perturbation alters the global radiative balance, through both the direct and semidirect aerosol effects. Indirect effects, i.e., changes to cloud albedo and lifetime due to interactions between aerosols and cloud droplets, are not treated. This makes it possible to extract, to our knowledge for the first time, the vertical profile of the semidirect effect of BC in isolation. Results will be shown for both a model setup where sea surface temperatures were held fixed and where a slab ocean was allowed to respond to the perturbation.

In the next section, we briefly present the CAM4 model, the simulations performed, and the methods used to extract the radiative flux changes due to the direct and semidirect effects. Then we present the main results before discussing the processes underlying the observed changes and how they compare to other recent studies.

2. Methods

This study was performed using the Community Atmosphere Model version 4 (CAM4) [*Neale et al.,* 2010], as the atmospheric component of the NCAR Community Earth System Model (CESM) version 1.0.3, run with a horizontal resolution of 1.9°×2.5° and 26 layers in the vertical dimension. The model top is at 3 hPa or approximately 40 km. The model was coupled to the Community Land Model version 4 [*Lawrence et al.*, 2011] and to an ocean component with either fixed sea surface temperatures (fSSTs) or a slab ocean model (SOM) [*Danabasoglu and Gent*, 2009; *Gent et al.,* 2011; *Kiehl et al.,* 2006]. For the fSST runs, the model internal climatology was used and was the same for all simulations. The fSST setup prohibits significant global mean temperature change while retaining fast atmospheric responses like the semidirect effect. For the SOM case, the model uses mixed layer temperatures from a preset control run. The global average mixed-layer depth is 54 m. Open-ocean parameterization is taken from *Hansen et al.* [1984] and is coupled to a thermodynamic model of sea ice. See *Neale et al.* [2010] for details. The CESM SOM produces a SST climatology consistent with that from a full ocean simulation [*Danabasoglu and Gent*, 2009]. Within reasonable limits, the fSST and SOM models used have been found to produce comparable cloud and precipitation responses [see, e.g., *Kvalevag et al.,* 2013].

Our CAM4 setup employed a bulk aerosol scheme, with number concentrations calculated from aerosol loadings assuming a single size. Hydrophobic and hydrophilic BC fractions are emitted and treated separately, but no aging of BC is performed. BC is also assumed to be fully externally mixed. BC optics are taken from the Optical Properties of Aerosols and Clouds data set [*Hess et al.,* 1998].

In CAM4, no direct aerosol modification of cloud properties are allowed, and hence, aerosol indirect effects are not represented. Semidirect effects, defined as the change in cloudiness due to the decrease in relative

humidity and increase in atmospheric stability caused by absorbing aerosol particles below, within, or above a cloud [see, e.g., *Jacobson*, 2012], are, however, fully present. Cloud burnoff, i.e., the effect of local heating on hydrometeors, is only included insofar as the CAM4 prognostic single-moment microphysics takes local temperature into account [*Rasch and Kristjansson*, 1998] but not through embedding of BC particles in or between hydrometeors.

Our aim was to investigate the atmospheric response to the insertion of a known quantity of BC aerosol globally at a given altitude. As previously shown, BC perturbs the climate on two time scales [*Andrews et al.,* 2010; *Kvalevag et al.,* 2013]. It alters atmospheric stability through local warming by absorption of solar radiation, inducing changes to precipitation that scale with the total amount of absorption added through the atmospheric column. These changes occur on short time scales, equilibrating during the first year after the perturbation. Further, BC increases global surface temperatures on slower time scales, similar to the response to a greenhouse gas. Atmospheric changes induced by this effect scale with the total top-of-atmosphere flux perturbation induced by the change in BC concentration.

To investigate both of these effects, two separate sets of model runs were performed. The model initial condition was a preequilibrated state with aerosol and greenhouse gas concentrations representative of year 2000. In both sets of runs, an additional constant burden of 3.0 mg m^{-2} BC was systematically added to a single model layer. As the model layers are of nonuniform depth, this was achieved by calculating and adding the volume concentration required to set the desired column burden. The model was then run to new stability. Changes were evaluated relative to an unperturbed control simulation. For practical purposes, we equate a single model layer with a given mean altitude, even though this is not strictly correct for the model layers nearest the surface. This does not significantly affect the interpretation of the results.

For the fast changes, we used the fSST configuration to prohibit responses in surface temperature. Twenty-seven 6 year runs were performed, one for each model layer, in addition to the baseline. Model equilibration was reached within the first simulation year. Atmospheric responses were then extracted as the mean of simulation years 2–6.

For changes that include responses in surface temperature, a SOM ocean setup was used, where the upper 54 m (on average) of the ocean were allowed to respond. Fourteen simulations of 30 years were run, one for every second model layer in addition to a baseline. Atmospheric responses were extracted as the means of simulation years 20–30 to ensure that the slab ocean had time to equilibrate. The BC perturbations used were the same for both sets of runs.

Additionally, we checked the linearity of the responses by also simulating lower burdens, between 0.1 and of 1.5 mg m^{-2}, at selected layers. No significant deviations from a linear response were found; hence, this sensitivity test is not discussed further.

Below, we will show both the RF from the direct aerosol effect and the semidirect forcing. The total atmospheric radiative response to the insertion of a layer of aerosol can be decomposed as follows:

$$\Delta F^{\mathrm{TOA}} = F_{\mathrm{Sig}} - F_{\mathrm{base}} = F^{\mathrm{SW}}{}_{\mathrm{Sig}} + F^{\mathrm{LW}}{}_{\mathrm{Sig}} - F^{\mathrm{SW}}{}_{\mathrm{Base}} - F^{\mathrm{LW}}{}_{\mathrm{Base}} \quad (1)$$

where F^{TOA} denotes the top of atmosphere downwelling radiative flux in W m^{-2}. SW denotes shortwave, or solar, radiation, and LW denotes longwave, or thermal, radiation. F_{Base} (baseline) refers to a simulation with BC concentrations representative of year 2000. F_{Sig} (signal) refers to a situation where BC has been added in a given model layer.

We wish to diagnose this response in terms of the aerosol direct shortwave radiative effect (hereafter labeled DRE) and the induced changes to temperature, clouds, humidity, etc. The latter is grouped together and labeled as the total aerosol semidirect effect ($\mathrm{SDE}^{\mathrm{TOT}}$). $\mathrm{SDE}^{\mathrm{TOT}}$ can be further divided into shortwave ($\mathrm{SDE}^{\mathrm{SW\text{-}CL}}$)and longwave ($\mathrm{SDE}^{\mathrm{LW\text{-}CL}}$) cloud responses, arising from a combination of changes in cloud fraction and cloud water content, and a residual flux change due to changes in temperature and humidity ($\mathrm{SDE}^{\mathrm{T,H2O}}$). These definitions allow us to rewrite equation (1) as

$$\Delta F^{\mathrm{TOA}} = \mathrm{DRE}^{\mathrm{SW}} + \mathrm{SDE}^{\mathrm{TOT}} = \mathrm{DRE}^{\mathrm{SW}} + \mathrm{SDE}^{\mathrm{SW\text{-}CL}} + \mathrm{SDE}^{\mathrm{LW\text{-}CL}} + \mathrm{SDE}^{\mathrm{T,H2O}} \quad (2)$$

where we have assumed that the longwave direct radiative effect of black carbon is negligible.

In the following, we follow the method and conventions set out in *Ghan et al.* [2013] to define the various radiative responses. To diagnose the DRE, we implemented a second radiation call in the CAM4 radiation scheme that excludes the shortwave radiative effects of aerosols. This diagnostic call was not allowed to influence the climate evolution. DRE can then be extracted as (omitting the SW index)

$$\mathrm{DRE} = \left(F_{\mathrm{Sig}}{}^{\mathrm{Aero}} - F_{\mathrm{Sig}}{}^{\mathrm{Clean}}\right) - \left(F_{\mathrm{Base}}{}^{\mathrm{Aero}} - F_{\mathrm{Base}}{}^{\mathrm{Clean}}\right) \tag{3}$$

CAM4 does not include treatment of the aerosol indirect effect, i.e., the modification of cloud properties by the aerosol particles. Hence, any additional changes in the top of atmosphere (TOA) SW flux beyond the DRE will be (mainly) due or changes in cloud fraction, in turn due to local heating or stability, change from the presence of BC, plus a (minor) modification due to shortwave absorption of water vapor. We equate this with the above defined shortwave aerosol semidirect effect:

$$\mathrm{SDE}^{\mathrm{SW\text{-}CL}} = \mathrm{F}^{\mathrm{SW,TOA}} - \mathrm{DRE} \tag{4}$$

The longwave TOA flux, however, will also be affected by changes in temperature and relative humidity. Again, following *Ghan et al.* [2013], we define the longwave aerosol semidirect effect as

$$\mathrm{SDE}^{\mathrm{LW\text{-}CL}} = \left(F^{\mathrm{LW,TOA}}{}_{\mathrm{AllSky,Sig}} - F^{\mathrm{LW,TOA}}{}_{\mathrm{ClearSky,Sig}}\right) - \left(F^{\mathrm{LW,TOA}}{}_{\mathrm{AllSky,Base}} - F^{\mathrm{LW,TOA}}{}_{\mathrm{ClearSky,Base}}\right) \tag{5}$$

Finally, $\mathrm{SDE}^{\mathrm{T,H2O}}$ is calculated from equation (2), as a residual, to complete the radiative budget.

In addition to the above statement, where applicable, we have diagnosed both the all-sky and clear-sky responses.

Introducing a layer of BC also affects precipitation. As discussed in, e.g., *Andrews et al.* [2010] and *Kvalevag et al.* [2013], precipitation change can be decomposed into a fast response due to changes in atmospheric stability and a slow response driven by a change in surface temperature. These responses may be radically different, especially for a locally warming (i.e., absorbing) component such as BC.

Below, we follow the convention of *Andrews et al.* [2010] and diagnose a total precipitation response ($\mathrm{dP}^{\mathrm{TOT}}$) from the slab ocean simulations. The fSST simulations, which prohibit significant global mean surface temperature change, are used to diagnose the fast precipitation change ($\mathrm{dP}^{\mathrm{Fast}}$). The slow, temperature-driven changes can then be extracted as

$$\mathrm{dP}^{\mathrm{Slow}} = \mathrm{dP}^{\mathrm{TOT}} - \mathrm{dP}^{\mathrm{Fast}} \tag{6}$$

3. Results

In the following, we first put our model results in context by presenting its response to the difference in BC concentrations between present-day and preindustrial conditions before moving on to the main results. We decompose and discuss the climate response to the insertion of a layer of BC at a given altitude, first for fSST and then for slab ocean. In both cases, we show the atmospheric vertical profiles of temperature, humidity, and cloud fraction. We then go on to discuss associated precipitation responses on fast and short time scales.

3.1. CAM4 Response in Context

To gauge the response of our model to a realistic perturbation, we ran two fSST simulations with BC aerosol concentrations set at present-day and preindustrial levels, respectively. Taking their difference allows us to extract direct and semidirect radiative forcings due to anthropogenic BC (from all sources), using the equations presented above. All numbers in this section are averages of years 2–36 of the simulations, i.e., a 35 year period after a 1 year equilibration time. This time period was used due to the relatively small perturbation applied.

Using its internal, climatological BC concentrations for years 2000 and 1850, CAM4 predicts an anthropogenic BC burden of 0.15 mg m^{-2} and an extinction coefficient of 11.1 m^2/g. The resulting shortwave direct radiative forcing, or DRE in the terminology above, is 0.17 W m^{-2}, yielding a forcing efficiency for BC of 1204 W/g. These values are consistent within one sigma uncertainties with the multimodel mean reported by the first phase of the AeroCom multimodel intercomparison [*Schulz et al.,* 2006]. They are also broadly consistent with the more recent phase II evaluation [*Myhre et al.,* 2013]; however, that publication did not evaluate the response to BC from all sources, but separated out its fossil fuel and biofuel components.

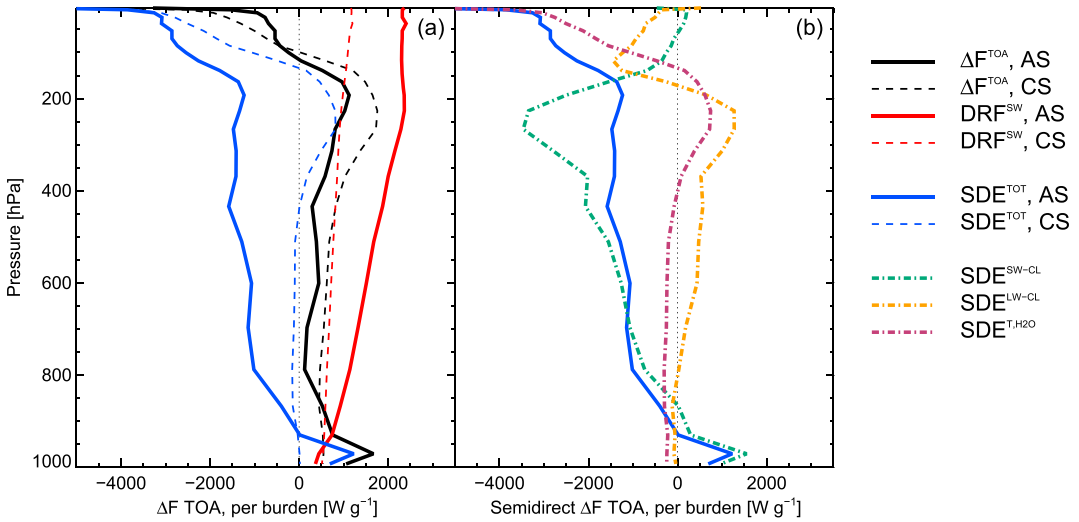

Figure 1. Vertical profiles of flux changes due to the insertion of a layer of BC aerosol at a given altitude. (a) Total flux change and direct and semidirect radiative effects. The dashed lines show clear-sky conditions. (b) Breakdown of the semidirect effect into longwave and shortwave cloud responses and a residual semidirect term due to changes in temperature and relative humidity.

The corresponding semidirect radiative forcing, or SDE^{TOT}, is −0.04 W m^{-2}, but with very large interannual differences, giving a standard deviation of 0.2 W m^{-2}. This range is mainly due to annual differences in the simulated cloud fraction, highlighting the importance of the cloud field representation, and its location relative to BC, for any estimate of the BC semidirect effect. The recent evaluation of BC climate effects by *Bond et al.* [2013] evaluated the total, all-effect semidirect effect of anthropogenic BC to be −0.1 W m^{-2}, with a 90% uncertainty range of (−0.30,+0.1) W m^{-2}, increasing to (−0.44,+0.1) W m^{-2} when accounting for possible reduction of high-altitude clouds from biomass-burning BC. The results of the present study fall well within the range of this evaluation. The large uncertainties still associated with the semidirect effect should be kept in mind for the discussion below. However, for a given consistent cloud representation and parameterization of BC effect, systematic evaluations of the response to BC in various locations are still highly instructive. For example, *Hodnebrog et al.* [2014] recently showed, using the same model as in the present work but different BC fields, how the net BC TOA RF can remain virtually unchanged under quite large, but realistic, emission perturbations, due mainly to the balancing impact of the semidirect effect.

3.2. TOA Flux Responses to BC

Figure 1 breaks down the total, fast, atmospheric radiative flux response, at TOA, to the insertion of a layer of BC at the pressure indicated on the ordinate. As the response is dependent on the amount of BC, all curves are normalized to the BC burden introduced (3.0 mg m^{-2}). All values are global averages of model years 2–6. Since we here prohibit surface temperature changes, Figure 1 should be interpreted as the sustained radiative flux perturbation from BC after the initial rapid adjustment from clouds, circulation, and humidity.

Figure 1a shows the net, i.e., shortwave (SW) plus longwave (LW), imbalance at top of atmosphere (TOA). From the surface and up to 100 hPa, we find a positive net flux change, which under our sign convention implies an accumulation of energy in the climate system. The flux change per burden peaks close to the surface, approaching 2000 Wg^{-1}, then stays between 500 and 1000 Wg^{-1} up to 100 hPa. At pressures below 100 hPa, the net flux change goes negative and strengthens sharply toward TOA.

To understand this total response, we study the various ways in which BC affects the atmosphere simulated in CAM4 by decomposing it as shown in equations (2)–(5) above. The solid red curve in Figure 1a shows the all-sky, direct, shortwave radiative effect from the layer of aerosols. It ranges from a weakly positive forcing close to the surface to a forcing stronger by around an order of magnitude at top of atmosphere. BC direct forcing efficiency increases for higher underlying albedo. Therefore, BC being located above clouds, and higher in the atmosphere with increasing importance of Rayleigh scattering, will enhance BC absorption. Further, lower in

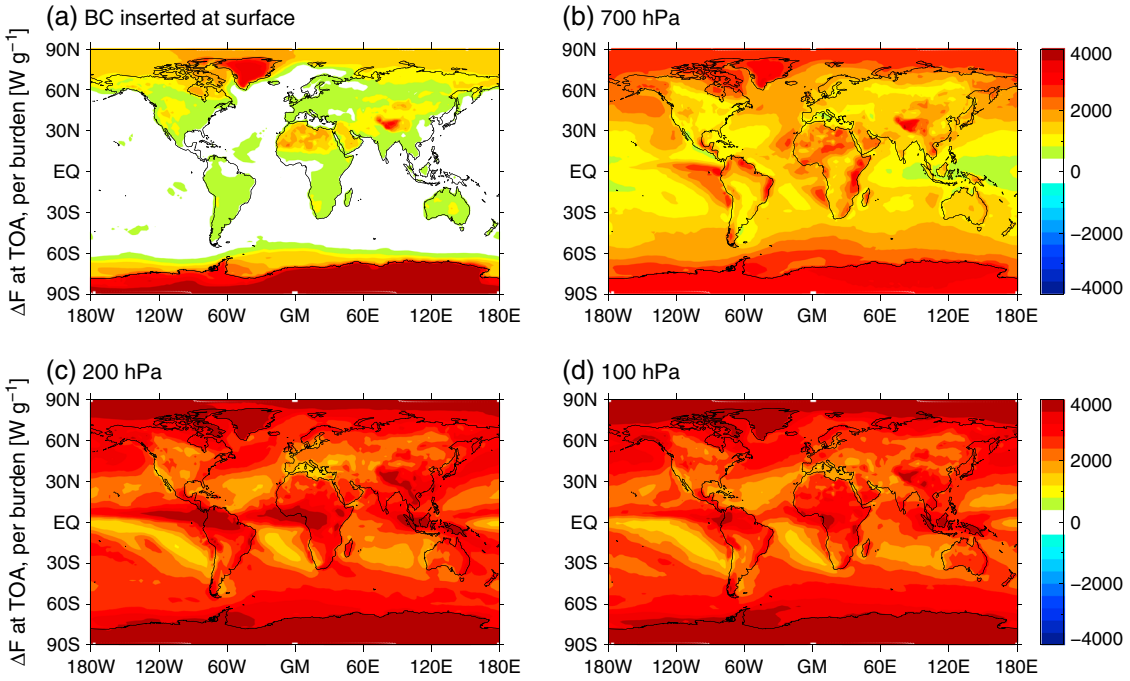

Figure 2. Annual mean maps of the all-sky aerosol direct radiative effect, per added aerosol burden, for black carbon inserted at four selected altitudes.

the atmosphere, some fraction of the incoming solar radiation is already absorbed by other absorbing components such as ozone and water vapor [*Samset and Myhre*, 2011]. (See Discussion below for a comparison of this curve with a previous study.)

The solid blue curve in Figure 1a shows the total semidirect atmospheric response (SDE^{TOT}). Since aerosols do not affect cloud properties directly in CAM4, this curve is the difference between the total response (black) and the direct aerosol perturbation (red). SDE^{TOT} is positive close to the surface but goes negative at 900 hPa. It continues to strengthen with altitude, opposing the positive flux perturbation from the direct effect.

The dashed lines in Figure 1a show the corresponding response in clear-sky conditions. The DRE at the surface is the same in both cases, but upward in the atmosphere, it is approximately halved relative to the all-sky case. This reflects the contribution of BC above clouds to the total DRE, a behavior consistent with what was found, e.g., in *Samset and Myhre* [2011], *Vuolo et al.* [2014], and *Zarzycki and Bond* [2010]. The parts of the SDE that arise from modification of clouds are naturally not present in clear-sky conditions. Hence, the clear-sky SDE is identical to the RSD perturbation shown in Figure 1b.

To diagnose SDE^{TOT}, Figure 1b decomposes it into $SDE^{SW\text{-}CL}$, $SDE^{LW\text{-}CL}$, and $SDE^{T,H2O}$ (as defined above). $SDE^{SW\text{-}CL}$ and $SDE^{LW\text{-}CL}$ are related to changes in cloud fraction and cloud thickness. For BC close to the surface, the SDE response is driven by $SDE^{SW\text{-}CL}$, arising from a decrease in low cloud fraction (see below). The decrease up toward 200 hPa is also driven by changes in SW flux. The LW flux change is modest near the surface but increases toward 200 hPa. Above 100 hPa, where the CAM4 cloud fraction vanishes, both the semidirect SW and LW perturbations tend toward zero. The residual flux perturbation ($SDE^{T,H2O}$), due to changes in temperature and humidity, is negligible up to 400 hPa. Between 400 hPa and 200 hPa, it gives rise to a positive TOA flux change, while at altitudes above 200 hPa, it is the cause for the strong negative trend seen in the total flux change. The latter is due to increased thermal emission from higher temperatures caused by absorbed solar radiation and thus enhancing the thermal cooling to space. Between 200 hPa and 400 hPa, the $SDE^{T,H2O}$ arises from a combination of the high altitude heating effect and changes to relative humidity through the atmospheric column. (See further discussion below.)

It is instructive to study more deeply the model responses to inserted BC that lead to the various flux perturbations. In Figures 2–5, we present supplementary results that further explain the features found in Figure 1.

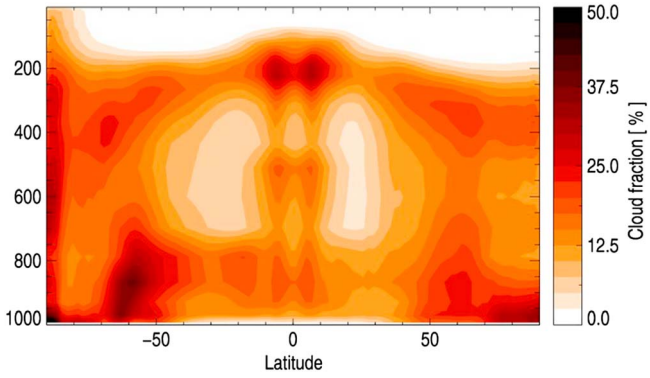

Figure 3. Annual mean cloud fraction field simulated by CAM4 from the baseline simulations used in the present work.

Figure 2 shows the geographical distribution of TOA direct RF efficiency for BC inserted at four selected altitudes. At the surface, BC is most efficient as a climate forcer over bright surfaces such as desert or ice. Greenland, the Himalayas, and the Antarctic are the only regions with significant forcing per gram from the direct effect. At 700 hPa, we start to see a larger contribution from areas with low-lying clouds, such as the regions west of Africa. At the highest altitudes, 200 hPa and 100 hPa, we can see a pattern in forcing per gram that is reminiscent of the global, annual mean cloud field in CAM4, modulated by high-albedo surface areas.

Going beyond the direct radiative effect of BC, we need to study changes to clouds. Figure 3 shows the zonal, annual mean distribution of cloud fraction in CAM4. A general global circulation pattern can be seen, with significant cloud fractions occurring in convection zones. We note that CAM4 predicts high cloud fractions close to the poles. In the Arctic, this is most pronounced close to the surface, while over the Antarctic, the high fraction extends all the way to 200 hPa. Above 200 hPa, cloud is mostly present above the equator. In the recent AeroCom phase II multimodel comparison, global mean cloud fraction was reported by 13 models [*Myhre et al.,* 2013]. The three CAM versions that took part all had cloud fractions consistent with the multimodel mean. However, a series of biases relative to measurements are known in the CAM4 cloud field [see, e.g., *Kay et al.,* 2012; *Williamson*, 2008]. The cloud field used is known to systematically underestimate the total cloud amount, overestimate the fraction of optically thick cloud, and underestimate midlevel clouds. All of these factors will impact the predicted climate response of BC, in particular, that of the semidirect effect. In

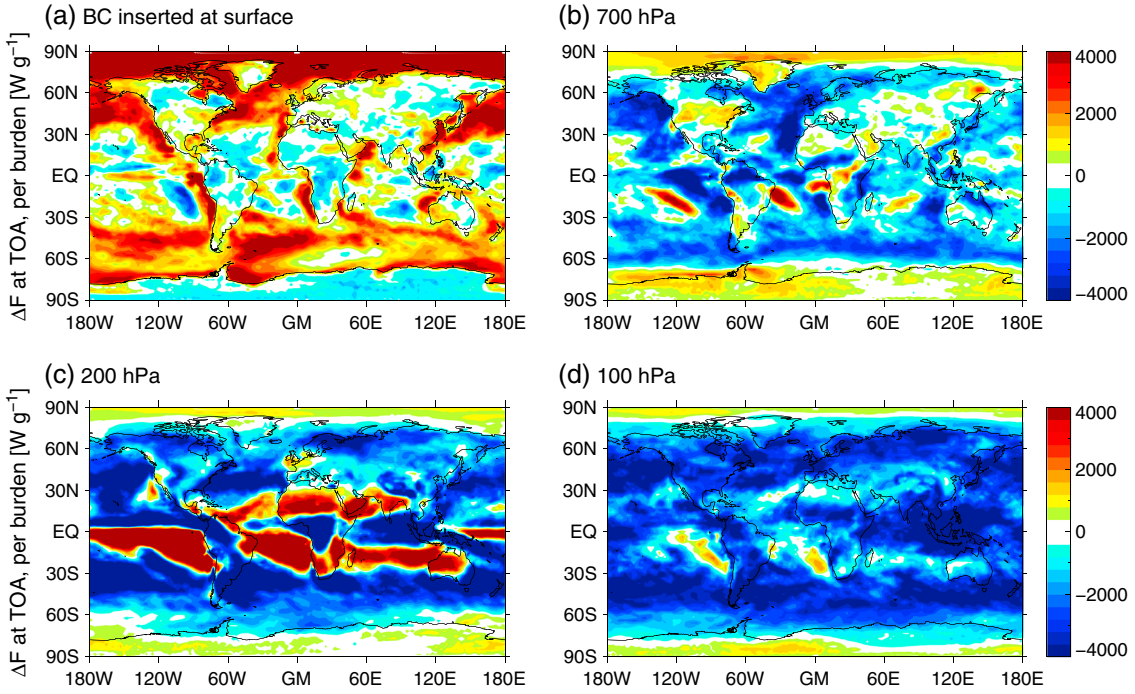

Figure 4. Annual mean maps of the total aerosol semidirect radiative effect, per added aerosol burden, for black carbon inserted at four selected altitudes.

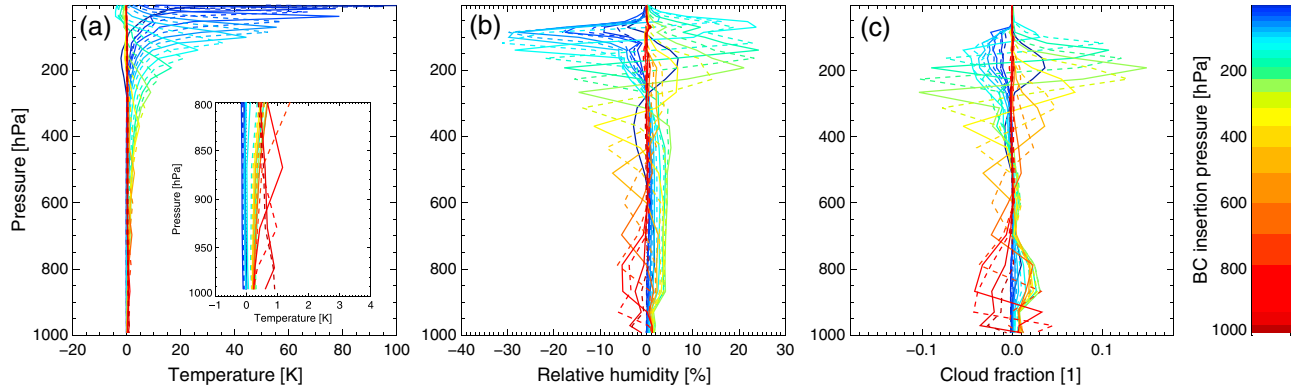

Figure 5. Altitude profiles of annual mean change in (a) temperature, (b) absolute humidity, and (c) cloud fraction for black carbon inserted at the altitude indicated by the profile color. Fixed SST condition profiles show the average response for simulation years 2–6 after the perturbation.

the present analysis, however, we take the CAM4 cloud representation as given and aim to repeat it using models with other cloud representations at a later stage.

Figure 4 shows comparable maps to Figure 2, for SDE^{TOT}. Here we see that the positive flux perturbation close to the surface, seen in Figure 1, comes mainly from the Arctic region and from the Southern Ocean. Over continents and over the Antarctic, BC at the surface leads to a negative semidirect flux perturbation. Therefore, the positive SDE^{TOT} seen at low altitudes in Figure 1 will only to a small extent be realized in CAM4 simulations with realistic emissions of BC. Emissions occur mainly over land, with transport over ocean mostly occurring at higher altitudes. At 700 hPa, there is a widespread TOA cooling due to SW reflection from an increase in cloud cover both above and below the layer where BC is inserted (see discussion of Figure 5 below). Referring to Figure 1, the response here is dominated by the $SDE^{SW\text{-}CL}$ term. At 200 hPa, we see some indications of BC causing an increase in high cloud fraction (see below), which introduces a positive $SDE^{LW\text{-}CL}$ in addition to the SW effect from increased albedo. At 100 hPa, we find globally uniform TOA cooling, due mainly to thermal reemission to space ($SDE^{T,H2O}$).

So far, we have discussed globally and/or annually averaged flux changes at TOA. In Figure 5, we show full vertical profiles of the response to each BC insertion, color coded from red at the surface to blue at the top model level (3 hPa). From left to right, we show the temperature response, relative humidity change, and change in cloud fraction. In Figure 5a, we note a strong temperature increase at pressures below 200 hPa, due to local heating from BC in a very dilute atmosphere. The resulting thermal cooling to space is the driving factor behind the strong $SDE^{T,H2O}$ close to TOA discussed above.

Figure 5b shows the impact of BC on the profiles of relative humidity (RH). BC between the surface and 500 hPa causes a local reduction in RH, with no effects at higher altitudes. Between 500 hPa and 100 hPa, we see a local reduction, accompanied by an increase at altitudes both above and below the insertion point. Above 100 hPa, there is again only a local reduction. In CAM4, the main mechanism for these changes in RH seems to be the local increase in temperature due to BC absorption, combined with changes in large-scale convection above and below the inserted layer.

Figure 5c, which shows changes to global, annual mean cloud fraction profiles, indicates a pattern very similar to that for RH. As noted for Figure 4 above, we find a marked increase in cloud fraction in subtropical ocean regions for BC inserted around 200 hPa. This corresponds to the location of absolute maxima in the CAM4 cloud field, seen in Figure 3, and to the peaks in both shortwave and longwave SDEs seen in Figure 1b. The increase in clouds leads to a marked increase in reflected shortwave radiation due to increased albedo (i.e., negative SDE) but also a strong longwave heating effect from high clouds (positive SDE). The net SDE at 200 hPa is, however, negative, indicating that for such an increase in cloud fraction, the shortwave interaction dominates the climate response.

Returning to Figure 4c, we can now, as an example, diagnose the regional pattern of SDE^{TOT} for BC inserted at 200 hPa. This total cloud field change is composed of a range of changes through the vertical column,

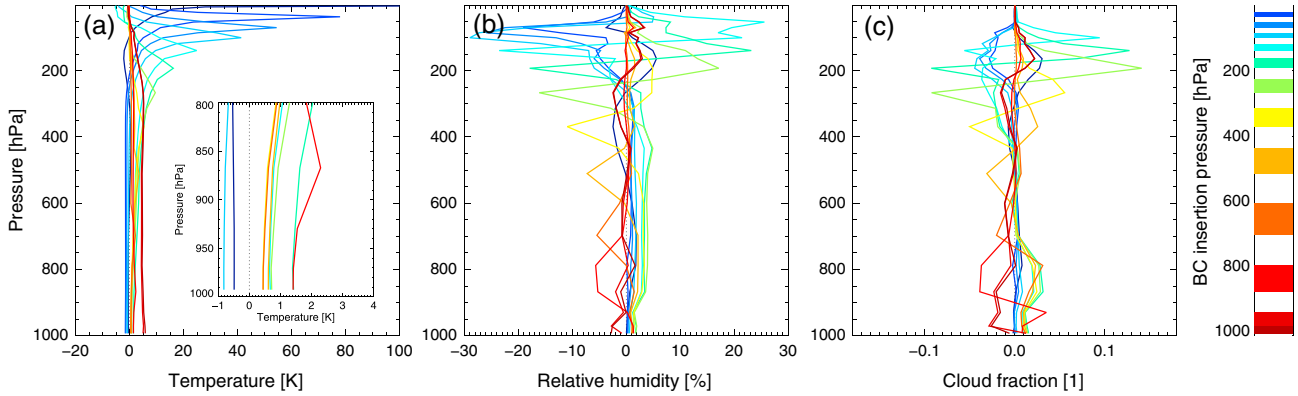

Figure 6. Altitude profiles of annual mean change in (a) temperature, (b) absolute humidity, and (c) cloud fraction for black carbon inserted at the altitude indicated by the profile color. Slab ocean condition profiles show the average response for simulation years 20–30 after the perturbation.

related to changes in the Hadley circulation in the model. Close to the ground, we see a small increase in cloud, due mainly to increased relative humidity in cloud formation regions (see Figure 3). At the layer where BC was inserted, a significant amount of cloud is removed due to local heating. This heated layer effectively becomes a new ceiling for the circulation. Below it, we find invigorated cloud formation around the equator but less cloud at midlatitudes due to reduced relative humidity. Above the layer, enhanced thermal instability leads to increased cloud fraction over most of the globe. We note, however, that as there is in reality very little BC at these altitudes [*Samset et al.,* 2014; *Schwarz et al.,* 2013], such a dynamical response will rarely be realized in nature.

3.3. Climate Response to BC

We now move on to results from simulations with a slab ocean component, i.e., where there is a response in surface temperature in addition to atmospheric circulation. The aim is to explore the sensitivity of the surface temperature precipitation responses to the presence of BC at a given altitude.

Twelve simulations were performed, where BC was inserted at a selected set of model layers. (We did not simulate every model level, as these simulations are more computationally expensive than the fSST cases due to significantly longer equilibration times.)

Figure 6 shows full vertical profiles of temperature, relative humidity, and cloud fraction for the slab ocean simulations, in the same format as Figure 5. The main differences to the fixed SST case are in the temperature response. BC causes a heating of the atmosphere where it is inserted, more efficiently toward higher altitudes due to the dilute air. However, note that BC inserted at levels above 200 hPa is found to have a cooling effect at the surface, due to the net reduction in radiation entering the tropospheric system.

In Figure 7a, we show the impact from BC inserted at a given altitude, on global, annual mean surface temperature, after equilibration of the slab ocean representation (mean of years 20–30 after the perturbation). As above, the perturbation is a 3 mg m^{-2} burden applied globally.

We find a strong heating from BC close to the ground, related to absorption by BC and altered thermal balance. Between 800 hPa and 100 hPa, we also find that BC is heating, though to a lesser degree for the same perturbation. Between 100 hPa and TOA, BC transitions into a cooling climate agent.

Figure 7b shows the corresponding precipitation response. BC inserted between the surface and 900 hPa is found to increase global precipitation due to increased low-level destabilization. At all altitudes above this point, the total, equilibrated precipitation impact of BC is negative, primarily due to increases in convective stability.

Precipitation response to BC occurs on two time scales. First, there is an almost instantaneous response from changes in atmospheric stability—in turn due to local heating. Then there is a slow, gradual response as the surface heats up. Both of these effects alter the hydrolocial balance. As described above, we can diagnose the fast changes from fSST runs, where surface temperature changes are prohibited and the total change from the slab ocean cases. The difference between these is the slow response (equation (6)).

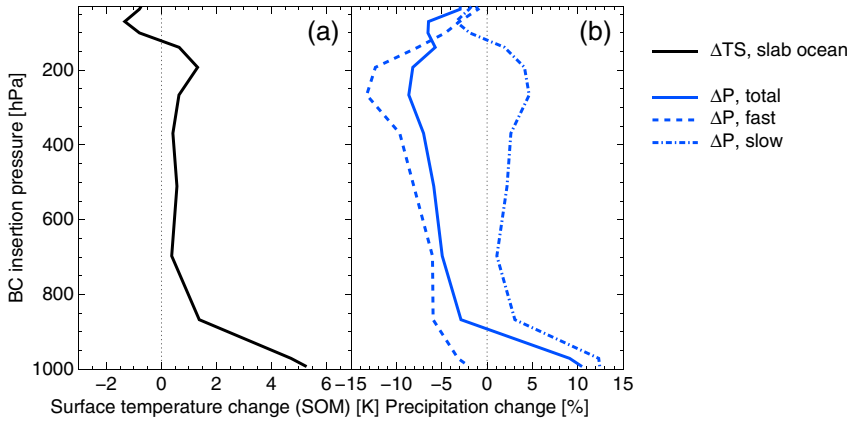

Figure 7. Global annual mean (a) surface temperature change and (b) precipitation change to a globally uniform burden of 3 mg m^{-2} added at the indicated altitude. The values shown are the global averages of years 20–30 after the perturbation in slab ocean conditions. Precipitation changes are decomposed into the total, fast, and slow responses as discussed in the text.

In Figure 7b, we break down dP^{TOT} from the insertion of BC into dP^{Fast} and dP^{Slow}. Here it becomes clear that the fast changes due to BC always act to decrease global mean precipitation, except above the troposphere. The slow, temperature-driven changes are always positive except at pressures below 100 hPa. The interplay between fast and slow changes gives the total pattern with an increase near the surface and a decrease in precipitation for BC higher in the atmosphere.

Our quite large perturbation of 3.0 mg m^{-2} was chosen to give significant responses throughout the atmospheric column. For the 10 year period used to extract the profiles in Figure 7, the year to year variability (one standard deviation) was 0.1 K and 0.5% for the temperature and precipitation profiles, respectively.

Moving beyond global mean results, and taking into account the fact that BC alters the radiative budget differently at different altitudes, we show global and zonal mean profiles normalized to the BC TOA flux perturbation and direct RF (Figures 8 and 9).

Figure 8a shows the surface temperature perturbation per unit of net TOA forcing. While the pattern is as in Figure 7a, we here clearly see that in terms of temperature impact per net flux change, BC is only relevant close to the surface. This is largely explained by the compensating, negative semidirect radiative effects discussed above.

Figure 8b breaks the global mean profile down zonally. For this plot, it is important to note that the BC perturbation at each atmospheric layer was applied globally. Hence, any impact on temperature may be due to a combination of local effects and changes due to impacts on large-scale circulation, e.g., as discussed in

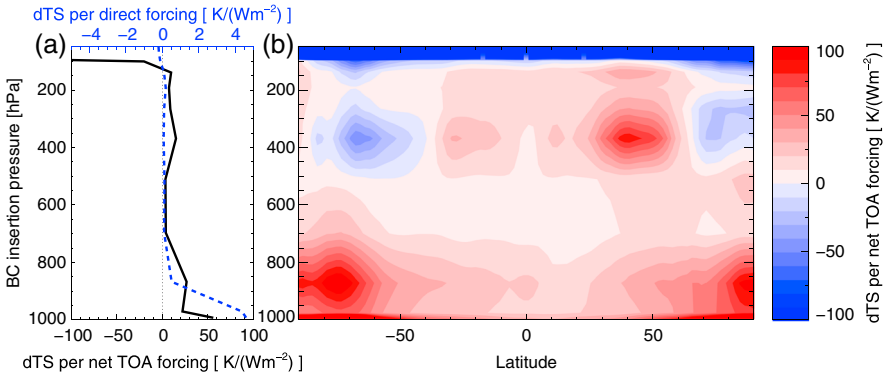

Figure 8. Temperature change per unit of net, TOA forcing from BC, as (left) global, annual mean profile (black) and as (right) zonal mean vertical structure. Also shown is the TOA forcing per unit of direct radiative forcing (left, blue dashed).

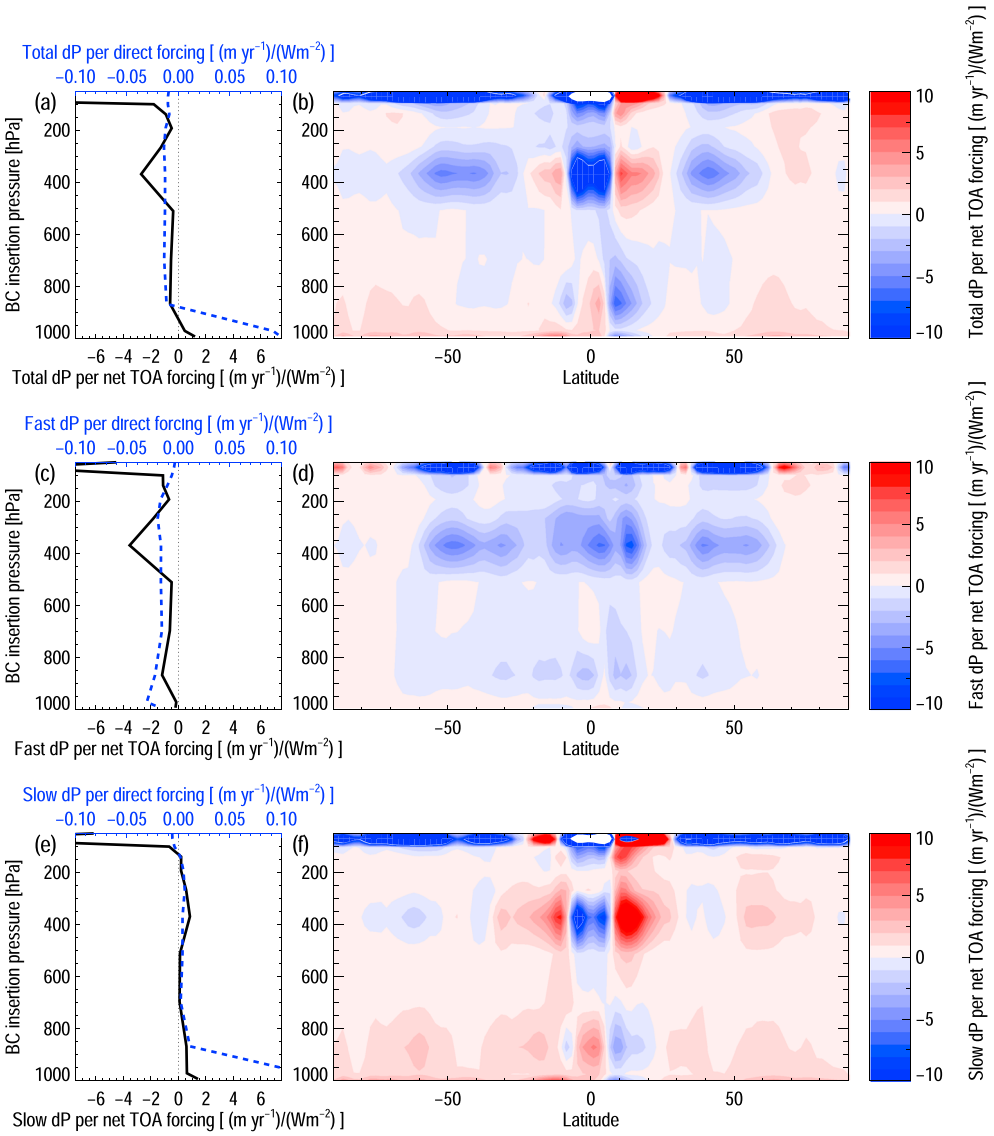

Figure 9. Precipitation change per unit of net, TOA forcing from BC, as (left) global, annual mean profile (black) and as (right) zonal mean vertical structure. Also shown is the TOA forcing per unit of direct radiative forcing (left, blue dashed). (top) Total precipitation change. (middle) Fast precipitation changes. (bottom) Slow precipitation changes.

relation to the semidirect effect above. The combined effect is that BC is most efficient as a heating agent close to the poles. The cooling effect at high altitudes is also found to occur mostly in the polar regions, except between 100 hPa and the TOA. Here BC effectively radiates absorbed energy back to space, leading to strong local, high-altitude heating (as shown in the profiles in Figures 5 and 6) but a cooling at the surface (as shown here). We note that for the region 80°N–90°N, BC inserted at $p < 500$ hPa leads to a net cooling, even though locally, both DRE and SDE are positive. This indicates the importance of assessing both local and remote BC impacts on polar temperature. Further simulations with regional perturbations, e.g., following the methods used in *Sand et al.* [2013] and *Flanner* [2013] are required to fully trace this response.

Recent literature on BC efficacy sometimes uses its surface temperature change per unit of direct radiative forcing, rather than total forcing [e.g., *Flanner*, 2013]. For comparability, Figure 8a also shows this metric. As for the response normalized to total forcing, the efficacy is strongest for BC close to the surface. However, the relative difference between surface and BC upward in the troposphere is stronger here. Hence, taking into account the semidirect effect reduces the efficacy correction that should be applied when predicting

surface temperature changes for BC aloft relative to the surface. Note also that surface cooling due to stratospheric BC is relatively much stronger per unit net forcing than per unit direct forcing.

Figures 9 shows similar plots for precipitation change (dP^{TOT}, dP^{Fast}, and dP^{Slow}). Looking first at the total, global mean response (Figure 9a), we recover the main trends seen in Figure 7. However, per unit TOA forcing, the precipitation response for BC inserted around 400 hPa is enhanced relative to near-surface BC.

Breaking the global mean response down into fast and slow components (Figures 9c and 9e), we see that on global mean and per unit TOA forcing, fast changes have a noticeable impact throughout the atmospheric column, while slow changes mostly appear close to the ground and at TOA. This is as expected as they are driven by surface temperature changes or a change in solar energy available for the atmospheric column.

However, Figures 9b, 9d, and 9f show a complex regional precipitation response pattern to BC forcing, beyond the global means. The total precipitation change is positive close to the surface at most latitudes but shows response to shifts in the Intertropical Convergence Zone (ITCZ) at higher altitudes. In a zone around 60°N–70°N, BC is found to increase precipitation at all altitudes except above 100 hPa. The reduction in precipitation from the fast response of BC is virtually global. An exception is BC at high altitudes over the polar regions, where a weak increase in fast response is found. The slow precipitation response is primarily positive, except around the equator and the ITCZ region.

4. Discussion

The situation described above, with 3.0 mg m^{-2} of BC added globally at a specified altitude, or model level, is unrealistic on two main counts. The amount of BC used is very large, in particular, at high altitudes where concentrations are normally quite low. We used this upscaled BC burden to achieve significant responses from the model, but interpretation of the results requires that the modeled response to BC insertion is relatively linear with burden. To test this, we performed tests with the entire present-day BC distribution multiplied by 10 throughout the column (see below) and with BC in a single layer increased by 0.3 mg m^{-2} and 1.5 mg m^{-2}. For all simulations, we extracted response parameters, such as forcing efficiency and extinction coefficients, and found them to be well consistent with the values presented above. We also confirmed that for perturbations of these strengths, the response in fSST for years 2–6, as used above, is consistent with the results from extended 30 year simulations.

Further, adding BC in a single layer may not invoke the same climate response as a more realistic vertical distribution. To test this, we calculated the DRE and SDE^{TOT} for the simulation with present-day BC multiplied by 10, both absolute and per unit burden, and compared these to the values found when scaling the response from individual layer perturbations to the realistic profiles. The results were consistent within 15%, indicating that for the fast responses, the above results are a useful basis for evaluating BC response also to other perturbations. We note, however, that this test cannot be expected to produce fully consistent results with a realistic perturbation. Ideally, simulations with regional perturbations should be carried out; however, this is beyond the scope of the present study.

Next, we need to consider the BC treatment in CAM4 relative to other models. Modeled climate response to BC depends, among other things, on the assumed radiative properties of the aerosol itself, the radiative transfer scheme, surface albedo, cloud distributions, and interactions with clouds. All of these factors vary between models. Hence, so will the response to a given amount and location of inserted BC. Conversely, similar experiments performed across models can be very instructive.

In *Samset and Myhre* [2011], the direct RF response to insertion of BC at a given model layer was presented. There, a pure radiative transfer scheme was used, combined with aerosol distributions from the OsloCTM2 chemical transport model. Results from that study are fully comparable to the direct BC RF in fSST simulations presented above.

Figure 10a shows a comparison of all-sky and clear-sky BC DRE^{SW} values from the two models. (Note that the OsloCTM2 results are updated relative to *Samset and Myhre* [2011], taking into account recent model improvements. The main characteristics are, however, very similar.) At first glance, the profiles are qualitatively similar. Regional DRE^{SW} patterns from OsloCTM2 are broadly similar to the CAM4 results shown here in Figure 2 (not shown). The two models, however, differ significantly in forcing strength.

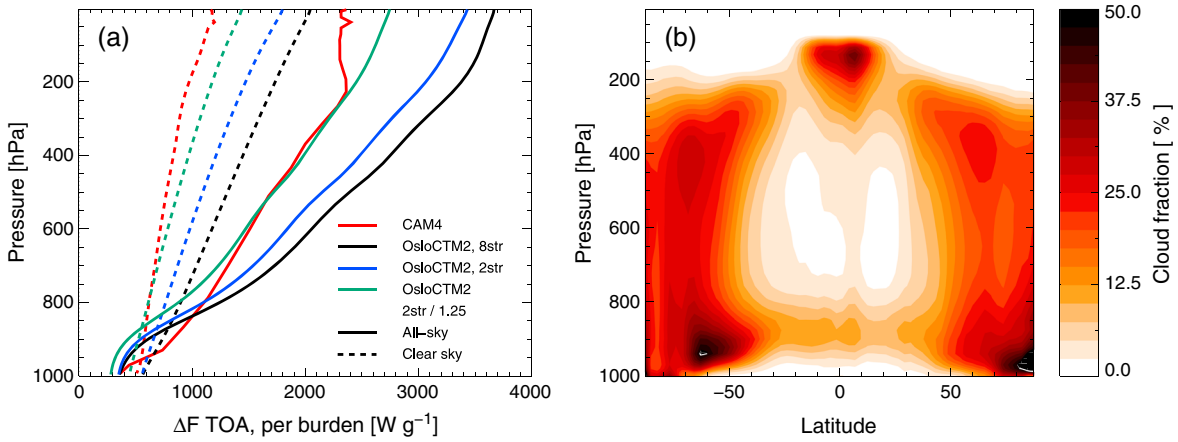

Figure 10. (a) Comparison of TOA BC direct radiative forcing efficiency as a function of BC altitude for CAM4 (red) and OsloCTM2 (black). Also shown are OsloCTM2 calculations with a two-stream radiative transfer scheme (blue) and where the latter has been reduced to remove a correction for BC aging (green). The solid lines show all-sky conditions; the dashed lines show clear-sky conditions. (b) Annual mean, zonal cloud fraction field used for the OsloCTM2 calculations.

There are several differences between the way the models have treated BC and its radiative interactions. First, the OsloCTM2 results are derived using an eight-stream radiative transfer model, while the radiation scheme in CAM4 is two-stream only. This was recently found to cause a 10% difference for global, annual mean modeled BC RF due to multiple scattering over high-albedo surfaces [*Myhre and Samset*, 2014]. For Figure 10a, we performed a calculation with the OsloCTM2 code in two-stream mode. The forcing strength can be seen to weaken, bringing the results closer to CAM4.

Further, the version of CAM4 used here does not treat aging of BC. This conversion process is known to enhance BC absorption by some factor [see, e.g., *Cappa et al.,* 2012], usually taken to be 50%. In the OsloCTM2 results, the added BC was assumed to be 50% hydrophilic and 50% hydrophobic. For the latter fraction, absorption was enhanced by 50%. (A similar enhancement was added, e.g., in *Flanner* [2013]). Removing this enhancement, by dividing the two-stream result by 1.25, yields a BC forcing efficiency for OsloCTM2 that is broadly consistent with the CAM4 results presented above.

Differences remain, however, close to the ground and at pressures below 200 hPa. These may be partly due to differences in surface albedo but are more likely related to differences in cloud representation. OsloCTM2 uses clouds from European Centre for Medium-Range Weather Forecasts reanalysis [*Myhre et al.,* 2009]. Figure 10b can be compared to Figure 3 above. At midlatitudes, CAM4 has a higher cloud fraction than OsloCTM2, which may explain the stronger BC forcing efficiency between 850 hPa and 950 hPa. High-altitude clouds above the ITCZ region are stronger in OsloCTM2, which may partly explain the difference at pressures below 200 hPa.

Figure 10a also shows clear-sky results. Even here, there is a clear difference in slope between the two models. Close to the surface, BC forcing strength is 10% weaker in OsloCTM2 than in CAM4, while at TOA, it is 15% stronger. This difference, consistent in magnitude with recent multimodel studies [*Randles et al.,* 2013; *Stier*, 2013], may be attributed, e.g., to differences in geographical location of BC relative to regions of high albedo, modeled relative humidity fields, optical properties of BC, and differences between the radiative transfer codes.

It is clear from the above that even the direct radiative interaction from BC aerosol is differently treated in present aerosol models. Since cloud fields are among the most poorly constrained elements of climate models, these differences can be expected to become even larger for estimates of the indirect and semidirect climate effects of BC.

A further limitation of the version of CAM used here is the lack of BC internally mixed with other species. For high-altitude BC in the polar regions, we find a TOA cooling, in line with a number of other studies with global circulation models. Studies focusing, e.g., on aircraft emissions, such as *Jacobson et al.* [2013], conversely find polar warming also at high altitudes. This has been interpreted as the effect of internal mixing of BC with

sulfate, enhancing its warming impact relative to externally mixed aerosol. The polar results found in the present study should hence be reevaluated using a model with more sophisticated treatment of BC mixing and optics.

For the semidirect effect, differences in cloud field representation have already been highlighted as a significant source of uncertainty. A further intermodel difference is the range of processes treated. For example, in *Bond et al.* [2013], the authors identify a possible additional contribution to the semidirect effect from BC inclusion in cloud droplets, with a separate climate forcing over the industrial era of +0.2 (−0.1, +0.9) W m^{-2}. This effect is not included in CAM4 and could result in significant changes to the results presented above.

5. Conclusions

We have presented the climate response to BC inserted at various altitudes in the atmosphere, under fSST and slab ocean conditions, as simulated by the NCAR CESM 1.0.3 climate model using the CAM4 atmospheric component. The direct radiative effect of BC is found to strengthen rapidly with altitude, consistent with a range of previous studies. The semidirect effect induced by BC is found to counteract the direct effect at all altitudes except near the surface. The net radiative flux perturbation to the presence of BC is found to be positive at all altitudes up to the tropopause but weak compared to the direct radiative effect alone. Above the tropopause, atmospheric BC acts to cool the surface, similar to other aerosol species such as sulfate, mainly due to strong reemission of absorbed sunlight. Similar to previous studies, we also find a globally applied BC perturbation to cause a net surface cooling in the polar regions, when present at atmospheric pressures below 500 hPa (altitudes greater than approximately 5 km). Significant amounts of BC at these altitudes are, however, also found to cause significant changes to large-scale circulation, relative humidity, and cloud formation. Further studies are required to separate the local polar temperature response from that from large-scale circulation changes. The precipitation response due to BC is found to have a fast component that is negative for all altitudes, due to an increase in atmospheric stability, but which over time is partly offset by a positive response to increased surface temperature and enhanced evaporation. After stabilization of a slab ocean setup, the net precipitation impact is positive for BC inserted between the surface and 900 hPa, due to a temperature-related increase in near-surface instability and negative for all other altitudes. The total precipitation response to BC in a climate model will therefore depend on its treatment of the lifetime and transport of black carbon.

Acknowledgments
This work was funded by the Norwegian Research Council through the grants SLAC, NAPEX, AC/BC and NetBC. All simulation data are available on request to the corresponding author (b.h.samset@cicero.oslo.no).

References

Allen, R. J., and W. Landuyt (2014), The vertical distribution of black carbon in CMIP5 models: Comparison to observations and the importance of convective transport, *J. Geophys. Res. Atmos.*, *119*, 4808–4835, doi:10.1002/2014JD021595.

Andrews, T., P. M. Forster, O. Boucher, N. Bellouin, and A. Jones (2010), Precipitation, radiative forcing and global temperature change, *Geophys. Res. Lett.*, *37*, L14701, doi:10.1029/2010GL043991.

Ban-Weiss, G. A., L. Cao, G. Bala, and K. Caldeira (2011), Dependence of climate forcing and response on the altitude of black carbon aerosols, *Clim. Dyn.*, *38*(5–6), 897–911, doi:10.1007/s00382-011-1052-y.

Bond, T. C., et al. (2013), Bounding the role of black carbon in the climate system: A scientific assessment, *J. Geophys. Res. Atmos.*, *118*, 5380–5552, doi:10.1002/jgrd.50171.

Boucher, O., et al. (2013), Clouds and aerosols, in *Climate Change 2013: The Physical Science Basis. Contribution of Working Group I to the Fifth Assessment Report of the Intergovernmental Panel on Climate Change*, edited by T. F. Stocker et al., pp. 571–658, Cambridge Univ. Press, Cambridge, U. K., and New York.

Cappa, C. D., et al. (2012), Radiative absorption enhancements due to the mixing state of atmospheric black carbon, *Science*, *337*(6098), 1078–1081, doi:10.1126/science.1223447.

Danabasoglu, G., and P. R. Gent (2009), Equilibrium climate sensitivity: Is it accurate to use a slab ocean model?, *J. Clim.*, *22*(9), 2494–2499.

Flanner, M. G. (2013), Arctic climate sensitivity to local black carbon, *J. Geophys. Res. Atmos.*, *118*, 1840–1851, doi:10.1002/jgrd.50176.

Gent, P. R., et al. (2011), The Community Climate System Model version 4, *J. Clim.*, *24*(19), 4973–4991, doi:10.1175/2011jcli4083.1.

Ghan, S. J., S. J. Smith, M. H. Wang, K. Zhang, K. J. Pringle, K. S. Carslaw, J. R. Pierce, S. E. Bauer, and P. J. Adams (2013), A simple model of global aerosol indirect effects, *J. Geophys. Res. Atmos.*, *118*, 6688–6707, doi:10.1002/jgrd.50567.

Hansen, J., A. Lacis, D. Rind, G. Russell, P. Stone, I. Fung, R. Ruedy, and J. Lerner (1984), Climate sensitivity: Analysis of feedback mechanisms, in *Climate Processes and Climate Sensitivity*, edited by J. E. Hansen and T. Takahash, pp. 130–163, AGU, Washington, D. C.

Hansen, J., M. Sato, and R. Ruedy (1997), Radiative forcing and climate response, *J. Geophys. Res.*, *102*(D6), 6831–6864, doi:10.1029/96JD03436.

Hansen, J., et al. (2005), Efficacy of climate forcings, *J. Geophys. Res.*, *110*, D18104, doi:10.1029/2005JD005776.

Hess, M., P. Koepke, and I. Schult (1998), Optical properties of aerosols and clouds: The software package OPAC, *Bull. Am. Meteorol. Soc.*, *79*(5), 831–844.

Hodnebrog, O., G. Myhre, and B. H. Samset (2014), How shorter black carbon lifetime alters its climate effect, *Nat. Commun.*, *5*, 5065, doi:10.1038/ncomms6065.

Jacobson, M. Z. (2012), Investigating cloud absorption effects: Global absorption properties of black carbon, tar balls, and soil dust in clouds and aerosols, *J. Geophys. Res.*, *117*, D06205, doi:10.1029/2011JD017218.
Jacobson, M. Z., J. T. Wilkerson, A. D. Naiman, and S. K. Lele (2013), The effects of aircraft on climate and pollution. Part II: 20-year impacts of exhaust from all commercial aircraft worldwide treated individually at the subgrid scale, *Faraday Discuss.*, *165*, 369–382.
Kay, J. E., et al. (2012), Exposing global cloud biases in the Community Atmosphere Model (CAM) using satellite observations and their corresponding instrument simulators, *J. Clim.*, *25*(15), 5190–5207.
Kiehl, J. T., C. A. Shields, J. J. Hack, and W. D. Collins (2006), The climate sensitivity of the Community Climate System Model version 3 (CCSM3), *J. Clim.*, *19*(11), 2584–2596.
Kipling, Z., P. Stier, J. P. Schwarz, A. E. Perring, J. R. Spackman, G. W. Mann, C. E. Johnson, and P. J. Telford (2013), Constraints on aerosol processes in climate models from vertically-resolved aircraft observations of black carbon, *Atmos. Chem. Phys.*, *13*(12), 5969–5986, doi:10.5194/acp-13-5969-2013.
Koch, D., et al. (2009), Evaluation of black carbon estimations in global aerosol models, *Atmos. Chem. Phys.*, *9*(22), 9001–9026, doi:10.5194/acp-9-9001-2009.
Kvalevag, M. M., B. H. Samset, and G. Myhre (2013), Hydrological sensitivity to greenhouse gases and aerosols in a global climate model, *Geophys. Res. Lett.*, *40*, 1432–1438, doi:10.1002/grl.50318.
Lawrence, D. M., et al. (2011), Parameterization improvements and functional and structural advances in Version 4 of the Community Land Model, *J. Adv. Model. Earth Syst.*, 3, M03001, doi:10.1029/2011MS00045.
Myhre, G. (2009), Consistency between satellite-derived and modeled estimates of the direct aerosol effect, *Science*, *325*(5937), 187–190, doi:10.1126/science.1174461.
Myhre, G., and B. H. Samset (2014), Standard climate models radiation codes underestimate black carbon radiative forcing, *Atmos. Chem. Phys. Discuss.*, *14*(19), 26,173–26,186, doi:10.5194/acpd-14-26173-2014.
Myhre, G., et al. (2009), Modelled radiative forcing of the direct aerosol effect with multi-observation evaluation, *Atmos. Chem. Phys.*, *9*(4), 1365–1392, doi:10.5194/acp-9-1365-2009.
Myhre, G., et al. (2013), Radiative forcing of the direct aerosol effect from AeroCom Phase II simulations, *Atmos. Chem. Phys.*, *13*, 1853–1877, doi:10.5194/acp-13-1853-2013.
Neale, R. B., et al. (2010), Description of the NCAR Community Atmosphere Model (CAM 4.0), *NCAR Tech. Note NCAR/TN-485+STR*, 212 pp.
Randles, C. A., et al. (2013), Intercomparison of shortwave radiative transfer schemes in global aerosol modeling: Results from the AeroCom Radiative Transfer Experiment, *Atmos. Chem. Phys.*, *13*(5), 2347–2379, doi:10.5194/acp-13-2347-2013.
Rasch, P. J., and J. E. Kristjansson (1998), A comparison of the CCM3 model climate using diagnosed and predicted condensate parameterizations, *J. Clim.*, *11*(7), 1587–1614.
Samset, B. H., and G. Myhre (2011), Vertical dependence of black carbon, sulphate and biomass burning aerosol radiative forcing, *Geophys. Res. Lett.*, *38*, L24802, doi:10.1029/2011GL049697.
Samset, B. H., et al. (2013), Black carbon vertical profiles strongly affect its radiative forcing uncertainty, *Atmos. Chem. Phys.*, *13*(5), 2423–2434, doi:10.5194/acp-13-2423-2013.
Samset, B. H., et al. (2014), Modeled black carbon radiative forcing and atmospheric lifetime in AeroCom Phase II constrained by aircraft observations, *Atmos. Chem. Phys. Discuss.*, *14*(14), 20,083–20,115, doi:10.5194/acpd-14-20083-2014.
Sand, M., T. K. Berntsen, J. E. Kay, J. F. Lamarque, O. Seland, and A. Kirkevag (2013), The Arctic response to remote and local forcing of black carbon, *Atmos. Chem. Phys.*, *13*(1), 211–224.
Schulz, M., et al. (2006), Radiative forcing by aerosols as derived from the AeroCom present-day and pre-industrial simulations, *Atmos. Chem. Phys.*, *6*, 5225–5246.
Schwarz, J. P., B. H. Samset, A. E. Perring, J. R. Spackman, R. S. Gao, P. Stier, M. Schulz, F. L. Moore, E. A. Ray, and D. W. Fahey (2013), Global-scale seasonally resolved black carbon vertical profiles over the Pacific, *Geophys. Res. Lett.*, *40*, 5542–5547, doi:10.1002/2013GL057775.
Stier, P. (2013), Host model uncertainties in aerosol radiative forcing estimates: Results from the AeroCom prescribed intercomparison study, *Atmos. Chem. Phys.*, doi:10.5194/acp-13-3245-2013.
Vuolo, M. R., M. Schulz, Y. Balkanski, and T. Takemura (2014), A new method for evaluating the impact of vertical distribution on aerosol radiative forcing in general circulation models, *Atmos. Chem. Phys.*, *14*(2), 877–897, doi:10.5194/acp-14-877-2014.
Williamson, D. L. (2008), Convergence of aqua-planet simulations with increasing resolution in the Community Atmospheric Model version 3, *Tellus, Ser. A*, *60*(5), 848–862.
Zarzycki, C. M., and T. C. Bond (2010), How much can the vertical distribution of black carbon affect its global direct radiative forcing?, *Geophys. Res. Lett.*, *37*, L20807, doi:10.1029/2010GL044555.